

**SYNTHESES and CHARACTERIZATIONS of
BIOINSPIRED COMPOSITES with REGENERATION
CAPABILITY**

By

Decheng Hou

A thesis submitted to Johns Hopkins University in conformity with the
requirements for the degree of Master of Science in Engineering.

Baltimore, Maryland
January 2020

© 2020 Decheng Hou
All rights reserved

Abstract

The objective of this research is to investigate synthetic pathways for bioinspired materials with regeneration ability. This study is a part of a larger study on bioinspired composites motivated by current challenges of synthetic structural materials, such as fixed mechanical properties and degradation over time. To address these challenges, we are inspired by natural materials such as bones and coral reefs that can adapt to their environment and regenerate.

Built upon previous findings that negatively charged scaffolds serve as templates for mineral formation from the medium with ions by attracting positive mineral ions, we hypothesized that if we use a scaffold with negatively charged surfaces, the damage of the mineralized scaffold will expose underlying negative charges so that it can provide “signals” for inducing mineral deposition, thus repairing the damaged mineral layer.

To test the hypothesis, we utilized piezoelectric materials that convert mechanical loading into electrical charges as scaffolds. After forming minerals by immersing into a simulated body fluid (SBF) that mimics the ionic concentrations of human blood, we

damaged the parts of the minerals and re-immersed samples into the SBF. Then, we compared the thickness profiles of the minerals before and after re-immersing by using an optical profiler. We also studied the effects of different piezoelectric scaffolds such as Polyvinylidene fluoride and piezoelectric composite.

We found that the damaged areas were regenerated with minerals while more studies are needed for a quantitative understanding of the mechanism. We envision that our findings can contribute to developing novel synthetic materials with regeneration capability with applications including coatings for bone-implants and remineralization of teeth.

Primary Reader and Advisor: Sung Hoon Kang

Secondary Reader: Gist Croft

Acknowledgments

I am very grateful to my advisor, Professor Sung Hoon Kang, for showing me the field of bioinspired material, and for his guidance in this project and my master's study.

I am also very grateful to Prof. Santiago Orrego, Mr. Zhezhi Chen, and Ms. Urszula Krekora, who also had significant contributions to this project. Working in such a diverse team broadened my thoughts and opened my mind, which is a precious research experience in my life.

I also would like to offer my sincere thanks to Mr. Boliang Wu, Mr. Shichen Xu, Mr. Junjie Pan, Mr. Ian McLane, Ms. Valerie Rennoll, Mr. Lichen Fang, and Dr. Ozan Erol, who generously offered their supports and suggestions to help me complete this project.

Contents

Abstract	ii
Acknowledgments	iv
List of Tables	vii
List of Figures	viii
1 Introduction	1
1.1 Motivation for Materials with Regeneration Capability	1
1.2 Previous Study on Bioinspired Materials with Regeneration Ability	4
1.3 Bioinspired Mineralization	5
1.4 Our Hypothesis	6
1.5 Outline of Thesis	7
2 Synthesis Mechanism of Bioinspired Composite	8
2.1 Charge-Induced Mineralization in Simulated Body Fluid	8
2.2 Piezoelectric Materials	10
2.3 Synthesis Method	11
2.4 Conclusion	14

3 Factors and Conditions Studied for Mineralization	15
3.1 Piezo-Coefficient	15
3.1.1 Measurement Method.....	16
3.1.2 Equipment and Setting	17
3.1.3 Testing Results	19
3.2 Different Concentrated Simulated Body Fluids	19
3.3 pH Value.....	22
3.4 Conclusion	23
4 Characterizations of Bioinspired Composites	25
4.1 Surface Morphology.....	25
4.2 Chemical Composition Analysis	27
4.3 Testing Regeneration of Damaged Areas	30
4.4 Conclusion	32
5 Conclusion and Future Work.....	33
5.1 Summary of Current Work.....	33
5.2 Future Work.....	34
5.3 Perspectives of Our Bioinspired Composite	35
Bibliography.....	36
Biography	42

List of Tables

Table 1 Ion concentration of SBF in comparison with human blood plasma. Reprinted from Biomaterials, 22(14), 2007-2012 ^[17] , with permission from Elsevier.....	8
Table 2 Reagents and preparation order for 1L 1xSBF. Reprinted from Biomaterials, 27(15), 2907-2915 ^[20] , with permission from Elsevier.....	12
Table 3 Reagents and preparation order for 1L simplified 1xSBF. Reprinted from Chemical Engineering Journal, 137(1), 154-161 ^[21] , with permission from Elsevier	13
Table 4 Reagents and preparation order for 200mL improved 5xSBF. Reprinted from Biomaterials, 25(22), 5323-5331, ^[22] with permission from Elsevier.....	20
Table 5 Reagents and preparation order for 200mL improved 10xSBF. Reprinted from Chemical Engineering Journal, 137(1), 154-161, ^[21] with permission from Elsevier.....	20

List of Figures

Fig. 1 Comparison of natural and synthetic materials in aspects of (a) strength and stiffness (normalized by density) and (b) toughness and modulus. Reprinted by permission from Springer Nature. ^[3]	2
Fig. 2 Percentage of recycled and landfilled waste in 2017 in the US. Data is from Advancing sustainable materials management: 2017 fact sheet, from the United States Environmental Protection Agency. ^[5]	3
Fig. 3 Current types of self-healing methods: (a) capsule-based, (b) vascular, and (c) intrinsic methods. Image reused with permission of the rights holder, Annual Review, Inc. Republished with permission of Annual Reviews, Inc., ^[6]	4
Fig. 4 Scanning electron micrographs of the negatively polarized surface with crystal layer (left) and positively polarized surface without any minerals (right) after immersed in simulated body fluids. Reprinted with permission. ^[15] Copyright 1996 American Chemical Society.....	6
Fig. 5 Illustrations of chain conformation for α -PVDF, β -PVDF, and γ -PVDF. Reprinted from Progress in polymer science, 39(4), 683-706 ^[27] , with permission from Elsevier.	11
Fig. 6 Schematic illustrations of a general procedure of synthesizing bioinspired composite.	13
Fig. 7 Scanning electron microscopic images of mineral precipitation on the negatively charged surface (left) compared to deposition on the positively charged surface (Right).....	14
Fig. 8 The direction system in piezoelectric materials. Reprinted with permission. ^[43] Copyright 2018 John Wiley and Sons.....	16
Fig. 9 Schematic of Berlincourt method	17
Fig. 10 The schematic of a d_{33} measurement set-up	18
Fig. 11 The d_{33} measurement results of two different PVDF samples under 10Hz loading, prepared from the same original PVDF sheet, for an hour.	19

Fig. 13 Mineral layer thickness on the same substrate soaked in different concentrated simulated body fluids for the same period.....	21
Fig. 14 pH variation in 12 hours and illustrations of typical phenomena at different stages. Temperature and relative humidity are consistent.....	23
Fig. 15 Common morphologies of calcium phosphate researchers have discovered. These shapes are (a) irregular spheres, (b) spheres, (c) flowers, (d) porous spheres, (e) bowknots, (f) dumbbells, (g) needles, (h) sheets, (i) self-assembled nanorods, (j) rosettes, and (k) flakes. Reprinted from <i>Acta biomaterialia</i> , 9(8), 7591-7621, ^[36] with permission from Elsevier.....	26
Fig. 16 (a) Dense spherical mineral layer observed in previous studies from Kokubo et al. and Li et al.; (b) Dense spherical mineral layer observed in our study share the same morphology; (c) Flaky-shape mineral layer shown in previous research from Kobayashi et al. and Li et al; (d) Flaky-shape mineral layer shown in our study also has been discovered. Reprinted from <i>Biomaterials</i> , 27(15), 2907-2915, ^[20] with permission from Elsevier.....	27
Fig. 17 XRD analysis of deposited minerals on PVDF substrate.....	28
Fig. 18 EDS analysis of chemical elements in the deposited mineral layer formed from 1x, 5x, 10x simulated body fluids separately.....	29
Fig. 19 Schematic of testing regeneration of damaged areas.....	30
Fig. 20 An overview of the sample after damage (Top) and after healing (Bottom).	31
Fig. 21 Thickness measurement of the damaged area and non-damage area after damage (Black) and after healing (Red)	32

Chapter 1

Introduction

1.1 Motivation for Materials with Regeneration Capability

Material property control is a crucial and essential topic in material science since human beings started using tools from ancient times. Some scholars say that the history of human beings is a history of material science because the advances of technologies that push our society forward are correlated with the discoveries of new materials. Ferguson ^[1] pointed out that human historical epochs are defined by classical materials used by civilizations such as the Stone, Copper, Bronze, and Iron Ages, and thus the levels of innovation and standards of living are related with the available material technologies. Cohen et al. ^[2] also mentioned in his book, *Materials and Man's Needs*, that the increasing extravagance in the use of materials is one of the hallmarks of modern industrialized society, and he also stated that “Materials by themselves do nothing; yet without materials can do nothing”. It can be seen that there is a strong

connection between human society and material science and studying material properties and synthesizing new materials are always important topics in human history.

While there have been tremendous progresses in materials research, there are still challenges to realize some of the desirable characteristics of natural materials in synthetic materials. There are many methods to design and process materials to achieve required material properties, such as post-processing, synthesis of composite or compounds, etc. However, man-made materials cannot totally take the place of natural materials in aspects of properties and sustainability. Wegst et al. compared the difference in properties, such as stiffness, strength, modulus, and fracture toughness, between natural materials and man-made materials (Fig. 1) [3]. In addition, natural materials are environment-friendly with outstanding sustainability and they usually are made from low-cost ingredients via energy-saving method, compared to synthetic materials [4].

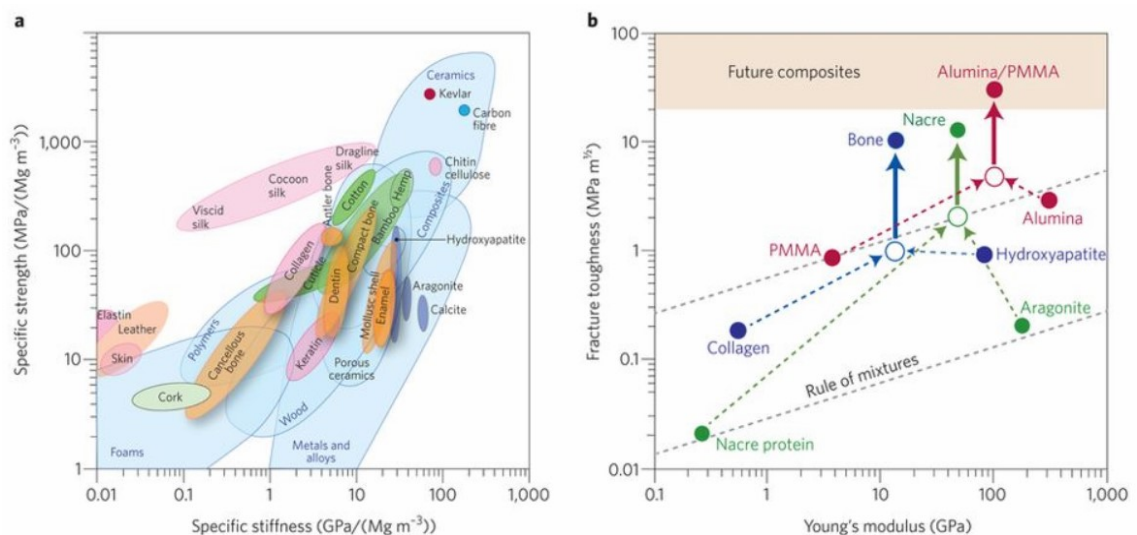


Fig. 1 Comparison of natural and synthetic materials in aspects of (a) strength and stiffness (normalized by density) and (b) toughness and modulus. Reprinted by permission from Springer Nature.^[3]

Thus, researchers have been studying to synthesize innovative materials that can

mimic natural materials like bones, silk, nacre, etc., not only to achieve unique material properties, but more importantly, to extend the lifecycle of synthesized materials and to explore new recycling methods for the future. The world-wide problem of lack of resources has been received public attention recently due to a large quantity of waste generated every year. According to a report from the United States Environmental Protection Agency ^[5], almost all materials people used in all aspects of life cannot reach a 50% recycling rate.

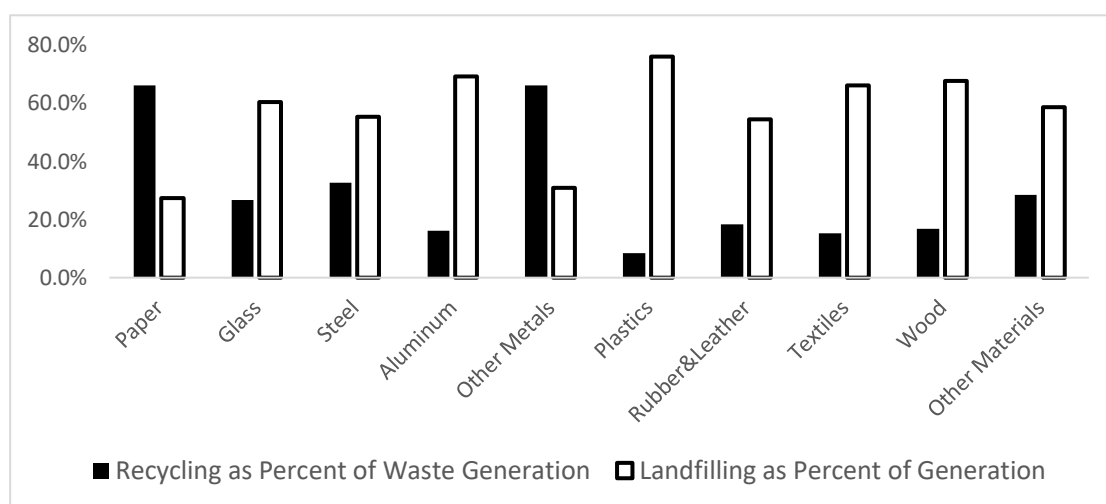


Fig. 2 Percentage of recycled and landfilled waste in 2017 in the US. Data is from Advancing sustainable materials management: 2017 fact sheet, from the United States Environmental Protection Agency. ^[5]

Besides recycling, another way to save resources is to enhance the lifetime of materials such as developing materials with regeneration capability, particularly in the case of medical implants where metals and plastics are common materials. Traditionally, medical implants usually need to be replaced periodically and cannot be reused due to the risk of biohazard and structure failure. Previously, researchers mainly focused on extending the period for replacement. However, no implants can be implanted forever like our bones, teeth, etc. If future implants can have regeneration capability, repairing their damage like bones, then it can not only reduce the expense and pain for patients

but also can be inspiring for people to explore novel methods in resource-saving and environmental protection.

1.2 Previous Study on Bioinspired Materials with Regeneration Ability

We are intrigued by properties of bones and consider bone as a model multifunctional material from nature. Previous research on repairing capability follows a similar pathway based on a review from Blaiszik et al., which are capsule-based healing systems, vascular healing systems, and intrinsic healing systems, as shown in Fig. 3. ^[6] Such materials can repair themselves by utilizing healing components embedded in itself.

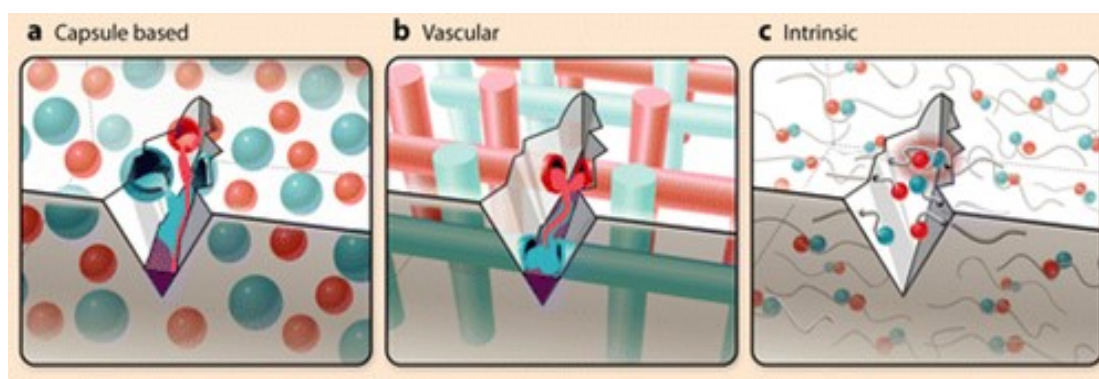


Fig. 3 Current types of self-healing methods: (a) capsule-based, (b) vascular, and (c) intrinsic methods. Image reused with permission of the rights holder, Annual Review, Inc. Republished with permission of Annual Reviews, Inc.;^[6]

There are many previous studies that correlate to these pathways and have made great progress in materials with regeneration capability. For instance, White et al. reported a capsule-based healing method, which can repair the crack via polymerization triggered by the release of healing agents and catalysts encapsulated and embedded in polymeric material ^[7]. Pang et al. demonstrated a self-repairing composite, containing

healing agents in composite's hollow vascular structure. The healing agents can infiltrate the damaged area and ameliorate its effect when it happens and breaks the vessel, similar to blood bleeding ^[8]. Chen et al. developed a polymeric material that can reconnect its fractured part by a simple heating and cooling method ^[9]. More recently, Li et al. reported a self-healing polymeric material that can self-repair at room temperature without any stimulus based on the re-formation of chemical bonds ^[10].

However, many of these previous healing mechanisms require an internal source of healing materials, which will be depleted and healing agents could be toxic. They also need special conditions for regeneration, which sometimes lead to a lack of biocompatibility for applications in medical implants. Our goal is to develop bone-inspired materials with regeneration capability, which are able to repair themselves by utilizing available raw materials around the damaged area.

1.3 Bioinspired Mineralization

Bone consists of about 40% inorganic components (primarily hydroxyapatite), 30% organic component (mostly collagen), and 25% water by volume ^[11]. Bassett et al. considered the collagen and apatite are the sources of piezoelectricity in bone and they may have special significance ^[12]. Noris-Suarez et al. reported that electrochemical action produced by piezoelectric dipoles generated from bone tissue can be the source of initial hydroxyapatite growth on the collagen substrate ^[13]. The further assumption stated that the electric fields formed by piezoelectricity from bone attract charged ions and macromolecules in the surrounding fluids, enhancing bone formation ^[14]. We are

inspired by the findings that bones are formed by mineralization of ions from body fluids onto charged scaffolds and they have signaling pathways to control the mineralization process.

Previous studies showed that minerals such as hydroxyapatite were preferentially deposited onto negatively charged surfaces from simulated body fluids (SBF), which is similar to those in human blood plasma. For example, Yamashita et al. reported rapid bone-like crystal growth on negatively polarized hydroxyapatite surfaces immersed in simulated body fluids (SBF) while they observed no crystal growth on positively polarized surfaces (Fig. 4) ^[15].

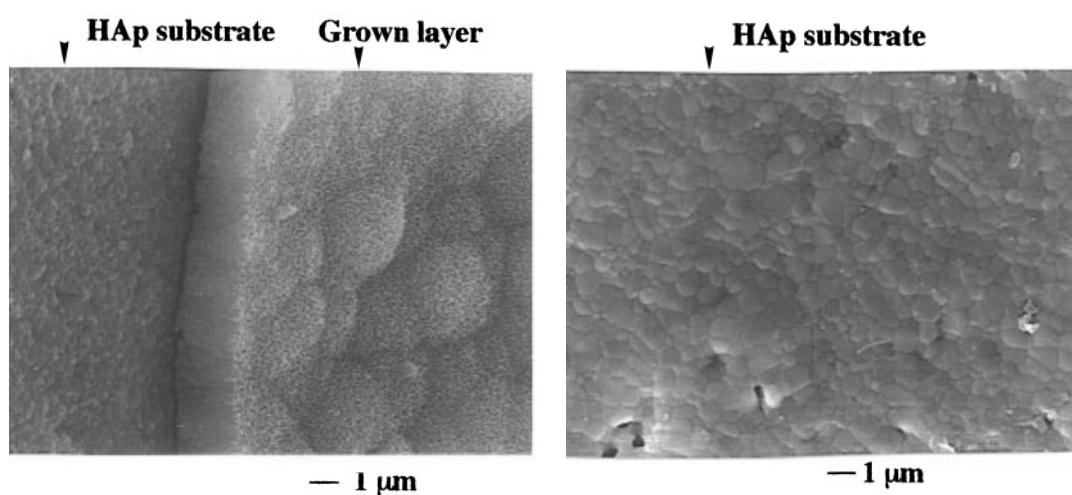


Fig. 4 Scanning electron micrographs of the negatively polarized surface with crystal layer (left) and positively polarized surface without any minerals (right) after immersed in simulated body fluids. Reprinted with permission.^[15] Copyright 1996 American Chemical Society.

1.4 Our Hypothesis

Built upon previous findings that negatively charged scaffolds serve as templates for mineral formation from the medium with ions by attracting positive mineral ions, we hypothesized that if we use a scaffold with negatively charged surfaces, the damage of the mineralized scaffold will expose underlying negative charges so that it can

provide “signals” for inducing mineral deposition, thus repairing the damaged mineral layer.

In addition, as piezoelectric materials generate charges, the use of a piezoelectric matrix can also provide excellent opportunities to understand the conditions, structures, chemical components, and regeneration capability based on mineral synthesis from simulated body fluids (SBF).

1.5 Outline of Thesis

The first chapter talked about the motivation for studying materials with regeneration capability, previous studies on regeneration mechanisms, studies on bioinspired mineralization, and our hypothesis. The second chapter will introduce our analysis about the mineralization mechanism based on the theory of crystallization, a brief introduction about the piezoelectric materials we used, and a general procedure for bioinspired composite synthesis. The third chapter will mainly focus on the factors and conditions we studied in the mineralization process. The fourth chapter will show our chemical analysis on our bioinspired composite and our current progress studying its self-regeneration capability. The fifth chapter will be conclusions, future work, and prospective applications of this project.

Chapter 2

Synthesis Mechanism of Bioinspired Composite

2.1 Charge-Induced Mineralization in Simulated Body Fluid

Simulated body fluid (SBF) is an acellular fluid with ion concentrations similar to those in human blood plasma ^[16] (Table 1^[17]), which normally contains soluble salts (KCl, NaCl, NaHCO₃, MgCl₂, CaCl₂, Na₂SO₄, phosphate salts) and buffer (Tris, HEPES, etc.).

Table 1 Ion concentration of SBF in comparison with human blood plasma. Reprinted from Biomaterials, 22(14), 2007-2012 ^[17], with permission from Elsevier.

	Concentration (mM)							
	Na ⁺	K ⁺	Ca ²⁺	Mg ²⁺	HCO ₃ ⁻	Cl ⁻	HPO ₄ ²⁻	SO ₄ ²⁻
SBF	142.0	5.0	2.5	1.5	4.2	148.5	1.0	0.5
Blood plasma	142.0	5.0	2.5	1.5	27.0	103.0	1.0	0.5

Mineralization in SBF traditionally is induced by carefully adjusting pH to achieve local supersaturation for mineral formation ^[18]. Supersaturation is a state of a solution that contains more solutes than it can dissolve without any precipitation. Under this

condition, when the solution slowly proceeds to the state of homogeneous nucleation but only a few nuclei start to grow, the starting crystallization will decrease the local ion concentration and bring the solution back into the region of supersaturation. Then, existing crystals will grow, but no new nuclei will form, which results in a slow but stable precipitation process. In 1990, Kokubo et al. first reported mineral formation on the surface of a glass-ceramic composite based on this method ^[19]. Since then, many researchers have used SBF to study mineralization for biomaterials in vitro and many revised versions of SBF have been created ^{[20][21][22]}. Despite the different versions of SBF, the precipitated mineral is commonly a form of calcium phosphate, which has been used as the coating layer for bone implants because calcium phosphate is one of the components of bones and it can be accepted by cells to reduce immunoreactions when implanted into the human body. Take hydroxyapatite, for example, the typical chemical reaction of precipitation in simulated body fluid is:



Generally, in the mineralization process, there are two crucial stages, which are nucleation and the growth of crystal nuclei. Nucleation is a phenomenon that tiny seed crystals start to form inside the solution. The rate of nucleation, J_N , is related to molar activation energy, Δg_n ^[23]:

$$J_N \propto e^{-\frac{\Delta g_n}{kT}}$$

where k is Boltzmann constant, and T is the temperature. The molar activation energy, Δg_n , is influenced by interfacial energy per area, σ , and local supersaturation factor, S_R :

$$\Delta g_n \propto \frac{\sigma^3}{(\ln S_R)^2}$$

And, in the case of hydroxyapatite precipitation,

$$S_R = \frac{[Ca^{2+}]^5 [PO_4^{3-}]^3 [OH^-]}{K_{SP}}$$

where K_{SP} is solubility product constant, and $[Ca^{2+}]$, $[PO_4^{3-}]$, $[OH^-]$ are molarity of ions or chemical groups. After nucleation, the formed nuclei begin to grow and accumulate on the substrate surface. The rate of crystal growth can be expressed in the form of power law ^[23]:

$$J_G = k(S_R - 1)^x$$

where J_G is rate of nucleation, S_R is relative supersaturation ratio, k is the rate constant, x is decided by step mechanism.

Based on the fundamental crystallization theory, we can speculate that the negative charges influence the crystallization of minerals in following aspects. Firstly, the negative charges increase the local relative supersaturation (S_R) of minerals by attracting calcium ions. The increase of S_R will result in the decrease of molar activation energy and then increase the nucleation rate. The increase of S_R will also lead to the increase of the crystal growth rate J_G . When crystal grows thicker, the influence of charges will decline, decreasing the crystallization rate.

2.2 Piezoelectric Materials

Due to the application of mechanical stresses, an electric charge can build up in a number of solid materials, including select ceramics, crystals and some biological materials like DNA, bone and certain proteins. The resulting effect is a type of

electricity produced because of pressure, known as piezoelectricity ^[24]. In 1880, the Curie brothers first demonstrated this phenomenon. Later, the converse effect was also discovered, in which a mechanical strain is generated by applying an electrical field ^[25]. Nowadays, there are many piezoelectric materials, both natural and synthetic. Some common natural piezoelectric materials are quartz, sucrose, bones, and wood, etc. ^[26]

In this study, we have used polymer-based piezoelectric materials such as polyvinylidene fluoride (PVDF). The piezoelectricity generated in polymers is caused by the molecular dipoles in the polymer chain and by the change of the dipole density in response to mechanical loadings. We used PVDF because it is a widely-used and commercially available piezoelectric polymer. The PVDF usually can be divided into three different types depending on its chain conformations, which are α -PVDF, β -PVDF, and γ -PVDF (Fig. 5) ^[27]. The β -PVDF was selected because of its good piezoelectric performance. Also, PVDF exhibits excellent chemical stability and is resistant to acids, weak bases, and ionic solutions, etc. ^{[28][29]}, which minimize other irrelevant reactions between PVDF and SBF.

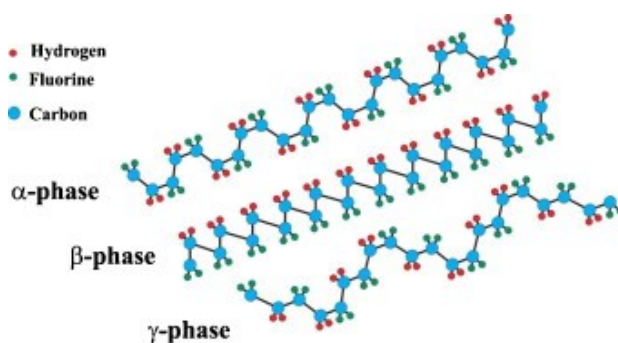


Fig. 5 Illustrations of chain conformation for are α -PVDF, β -PVDF, and γ -PVDF. Reprinted from Progress in polymer science, 39(4), 683-706 ^[27], with permission from Elsevier.

2.3 Synthesis Method

The first step of the composite synthesis is to prepare simulated body fluids (SBF).

We mainly followed recipes based on studies from Kokubo et al. (Table 2) and Yang et al. (Table 3).^{[20][21]} Kokubo et al. provided a very detailed procedure of SBF preparation in their published work. Well-prepared SBF should be preserved at 5-10°C and need to be used within 30 days^[20]. When preparing the SBF from Yang et al., we firstly prepared 1L distilled and ion-exchanged water (DI water) in a plastic bottle with a stirring bar. Then, we added chemicals following the order from the recipe shown in tables below; NaCl first, then KCl, CaCl₂·2H₂O, MgCl₂·6H₂O, NaH₂PO₄·H₂O, and finally stop dissolving chemicals when K₂HPO₄·3H₂O has been added. We only added the next chemicals when the previous one was totally dissolved. The solution prepared at this stage is called the stock solution, which can be stored in the fridge at 4°C for months. Every time before usage, the stock solution needs to be heated to 37°C in the incubator and then dissolve NaHCO₃. Then, the SBF should be used immediately because it does not have Tris to construct a buffer solution, thus, it cannot be stored too long after preparation.

Table 2 Reagents and preparation order for 1L 1xSBF. Reprinted from Biomaterials, 27(15), 2907-2915^[20], with permission from Elsevier.

Reagent	Order	Amount
NaCl	1	8.035 g
NaHCO ₃	2	0.355 g
KCl	3	0.225 g
K ₂ HPO ₄ ·3H ₂ O	4	0.231 g
MgCl ₂ ·6H ₂ O	5	0.311 g
1.0M HCl	6	39 mL
CaCl ₂	7	0.292 g
Na ₂ SO ₄	8	0.072 g
Tris	9	6.118 g
1.0M HCl	10	0-5 mL

Table 3 Reagents and preparation order for 1L simplified 1xSBF. Reprinted from Chemical Engineering Journal, 137(1), 154-161 [21], with permission from Elsevier

Reagent	Order	Amount
DI Water	0	1 L
NaCl	1	7.995 g
KCl	2	0.224 g
CaCl ₂ ·2H ₂ O	3	0.368 g
MgCl ₂ ·6H ₂ O	4	0.305 g
K ₂ HPO ₄ ·3H ₂ O	5	0.228 g
NaHCO ₃	6	0.349 g

Next, samples were prepared from a commercial PVDF film (TE Connectivity, PN: 3-1003352-0), slightly distorted to generate piezoelectricity, and were carefully placed into the SBF solution. The SBF solution should be refreshed every day to maintain the concentration based on a previous study showing the change of the ionic concentrations without refreshing [30]. After mineralization, the samples were repeatedly rinsed gently in the DI water to remove salts like NaCl. The salinity of the rinsing solution was measured by a salinity meter (Extech, EC170). When salinity was below 0.1 ppt, samples were taken out and dried at room temperature in air for further analysis. (Fig.

6)

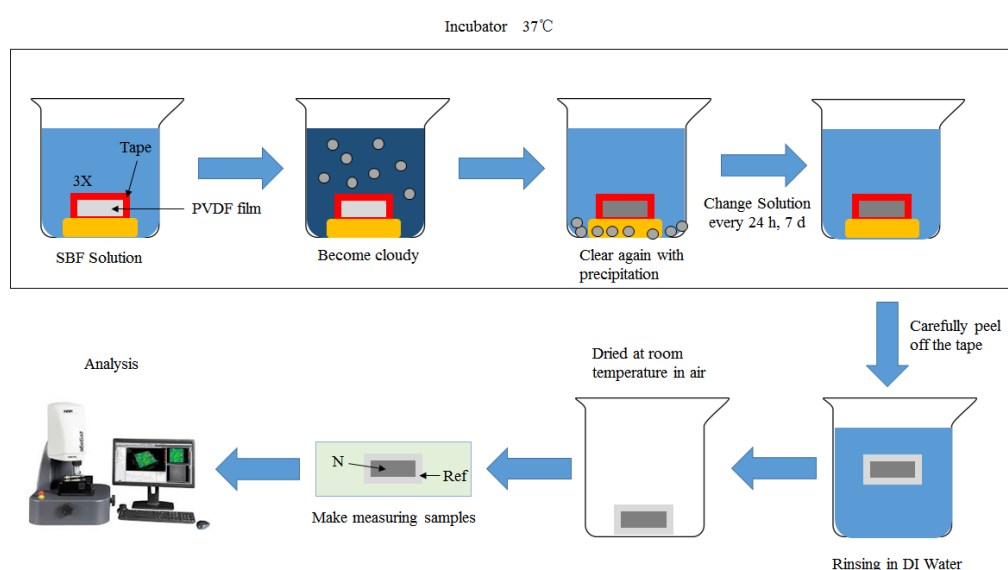


Fig. 6 Schematic illustrations of a general procedure of synthesizing bioinspired composite.

Later, samples were characterized by a profilometer (Laser Scanning Microscope, Keyence VK-X100, Osaka, Japan), X-ray diffraction (XRD; Philips, X'Pert Pro for powder), scanning electron microscope (SEM; Tescan, Mira3), and some other methods based on the purpose.

During our mineralization experiment, we noticed that the minerals were preferentially deposited on the negatively charged surface compared to the positively charged surface (Fig. 7). However, there are some other factors can also affect the mineralization process, such as concentration, time, loading conditions, and pH value, etc.

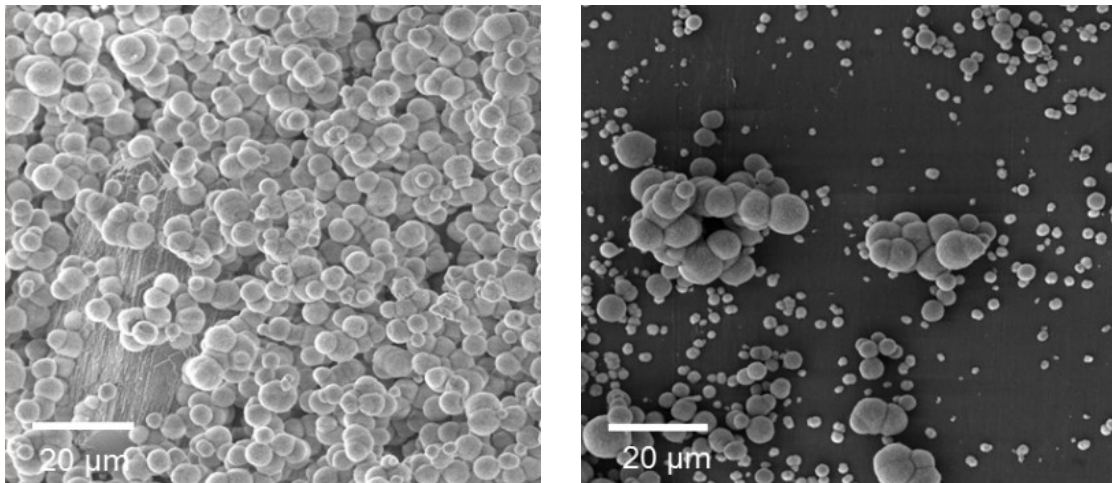


Fig. 7 Scanning electron microscopic images of mineral precipitation on the negatively charged surface (left) compared to deposition on the positively charged surface (Right).

2.4 Conclusion

In this chapter, we introduced the mineralization mechanism based on the theory of crystallization. We also described the piezoelectric materials we used and presented a novel mineralization method by utilizing piezoelectricity based on previous research on charge-induced mineralization. By using piezoelectric substrates, more minerals are precipitated on the negatively charged surface.

Chapter 3

Factors and Conditions Studied for Mineralization

3.1 Piezo-Coefficient

The piezocoefficient d_{ij} is the ratio of the charge per unit flowing along the j -direction to the stress applied in the i -direction and a typical unit is pC/N^[42]. There are different piezo-coefficients based on directions of polarization and applied mechanical forces to assess piezoelectricity in different situations. Usually, the piezoelectric coefficients are defined with double subscripts, with the first subscript indicating the direction of the electric field associated with the applied voltage/produced charge and the second subscript indicating the direction of the mechanical stress/strain^[31]. Direction X, Y, or Z is represented by the subscript 1, 2, or 3, respectively, and shear on one of these axes is represented by the subscript 4, 5, or 6, respectively.^[24] (Fig. 8)

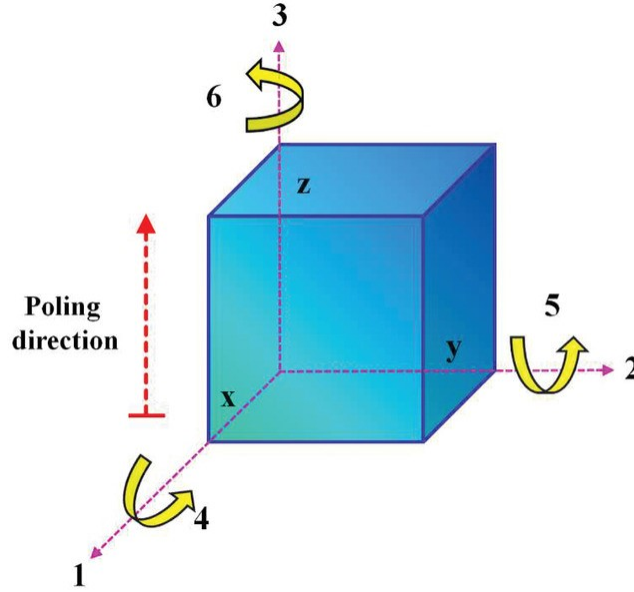


Fig. 8 The direction system in piezoelectric materials. Reprinted with permission.^[43] Copyright 2018 John Wiley and Sons.

In our case, the materials we used are PVDF films (TE Connectivity, PN: 3-1003352-0). Their direction of polarization is along the thickness direction, which is Z direction or 3 direction. As we are interested in mineralization on the film surface, the direction of generated electric field should also be along the thickness direction. To simplify our study, a basic loading pattern has been applied, such as uniaxial compression on the film. Thus, the relevant piezoelectric coefficient needs to be measured is d_{33} .

3.1.1 Measurement Method

The Berlincourt method ^[32] (also called the direct method) has been selected as our measurement method. When testing with Berlincourt method, a small oscillating force is applied to the testing sample and the measured charge output is divided by the oscillating amplitude (Fig. 9). This testing method is easy to set up and many commercial models, such as PM300 d_{33} PiezoMeter System (Manufactured by

Veginean Technology), are developed based on this mechanism due to its simplicity. However, since the system can be assembled by equipment from different manufacturers and there is no strict standard for calibration, the measurement results between different systems could produce a large variability ^[33]. In general, measurements are good within a batch or batch to batch, but the confidence in results from different systems could be much lower.^[32]

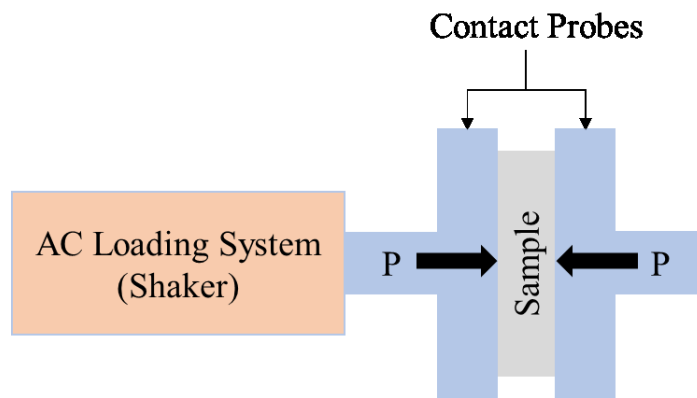


Fig. 9 Schematic of Berlincourt method

In our project, piezocoefficients were measured with the same testing system and each sample was tested multiple times. Besides, the purpose of measuring piezocoefficients is to learn the piezoelectric behaviors of our samples.

3.1.2 Equipment and Setting

In our piezo-coefficient measurement system, a synthesized function generator (SRS Model DS345) was used to generate an input signal by setting the wave type, amplitude in voltage, and frequency, to the power amplifier (APS Dynamics, Type APS 125), which is connected to the shaker (APS Dynamics, ELECTRO-SEIS APS 113 Shaker). The amplitude can be precisely monitored by a displacement sensor for adjustment. The shaker received the output signal from the amplifier and applies

dynamic force to a sample. The sample was under compression during measurement and the output charges were collected by piezo film lab amplifier (Measurement Specialties, P/N 1007214) via two copper electrodes connected to the sample. External forces are measured by a load sensor (LRM200, FUTEK). All information is processed by a data acquisition system (NI-PCI 6251 and BNC-2110, National Instruments, Texas) using LabVIEW 2013 (Fig. 10).

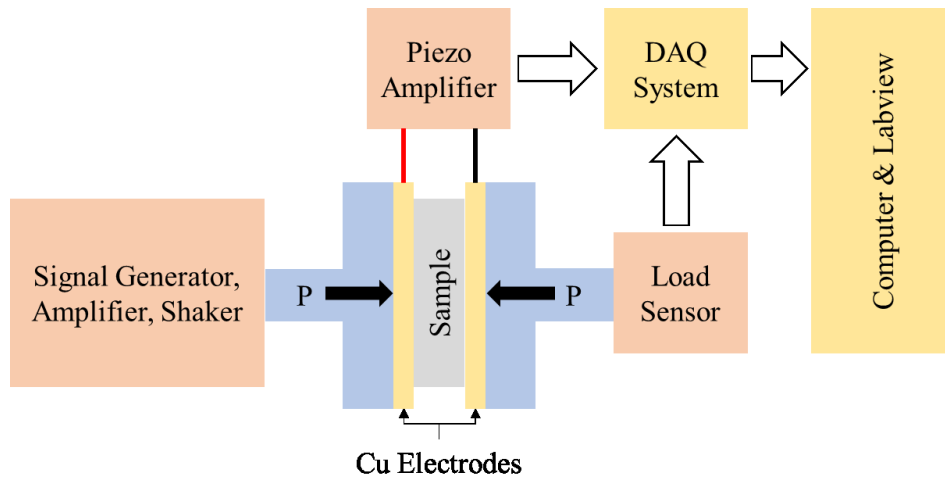


Fig. 10 The schematic of a d_{33} measurement set-up

Samples were carefully prepared to keep the dimension consistent ($2 \times 4 \text{ cm}^2$) and were stored at room temperature at least 24-hour before measurement to eliminate charges generated during preparation. When measuring d_{33} value, the testing conditions were: sine wave, 10 Hz, and 5 N dynamic loading (compression). Tests were set under relatively small loading and low-frequency environment because we would like to simulate the potential environment happened in an organism, especially in the human body, for future applications. However, there is a recommended lower limit for the Berlincourt method, which is around 10 Hz ^[33], according to the previous study. To ensure the stability and reliability of the measurement, we decided to utilize the setting

above and the d_{33} value of each sample was recorded for an hour.

3.1.3 Testing Results

Fig. 11 shows examples of data from two different PVDF specimens. It is clear that there is a time-dependent effect at the beginning, starting at a higher value and then gradually becoming stable afterward. One of the measured values was close to the reference d_{33} value provided by the manufacturer, which is 33 pC/N, but the other one was lower than the reference value. It is unclear why there is a difference between the measured value and the reference value. Though studies showed that the frequency, preload, time, and even geometry will influence the measurement of d_{33} value [33], we have carefully controlled these factors during measurements and we supposed influences based on these factors should be inhibited.

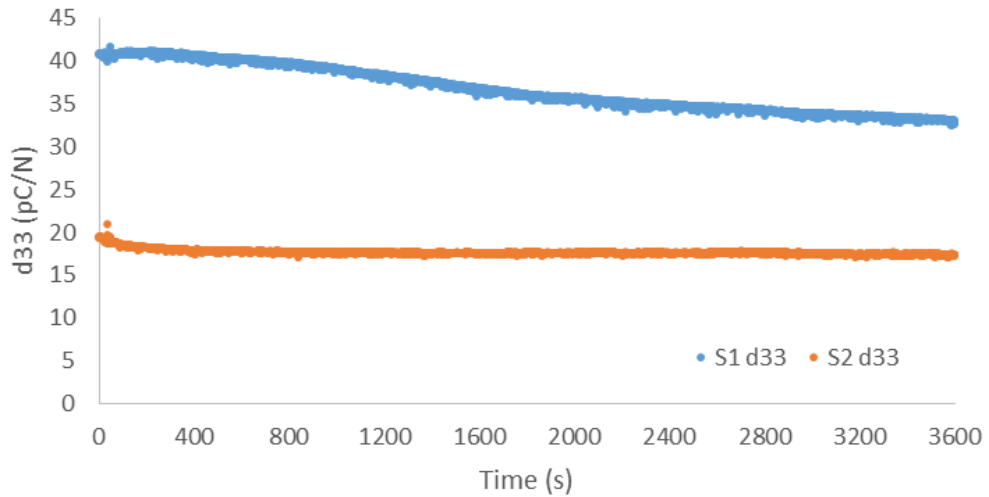


Fig. 11 The d_{33} measurement results of two different PVDF samples under 10Hz loading, prepared from the same original PVDF sheet, for an hour.

3.2 Different Concentrated Simulated Body Fluids

We investigated the contribution of simulated body fluids on the synthesis of

minerals onto PVDF films. The research can provide us a quantitative understanding of how we can tune the mineral deposition from the solution system. The simulated body fluid (SBF) solutions were prepared based on several previous studies ^{[20][21][22]}. Among them, Kokubo's recipe ^[20] of standard concentration SBF (1xSBF) is the most widely used one. They also provided several differently concentrated SBFs such as 0.5 times concentrated and 1.5 times concentrated solution. The mineral precipitation rate in 1xSBF is relatively low, which takes time to grow thick minerals for future measurements. Thus, we also referred to some other recipes (5xSBF and 10xSBF) ^{[21][22]}, shown in Table 4 and Table 5, which are derived from Kokubo's recipe, for faster mineralization and comparison.

Table 4 Reagents and preparation order for 200mL improved 5xSBF. Reprinted from Biomaterials, 25(22), 5323-5331,^[22] with permission from Elsevier.

Reagent	Order	Amount
DI Water	0	200 mL
NaCl	1	7.884 g
KCl	2	0.373 g
CaCl ₂ ·2H ₂ O	3	0.368 g
MgCl ₂ ·6H ₂ O	4	0.305 g
NaH ₂ PO ₄ ·H ₂ O	5	0.138 g
NaHCO ₃	6	0.353 g

Table 5 Reagents and preparation order for 200mL improved 10xSBF. Reprinted from Chemical Engineering Journal, 137(1), 154-161,^[21] with permission from Elsevier.

Reagent	Order	Amount
DI Water	0	200 mL
NaCl	1	11.686 g
KCl	2	0.075 g
CaCl ₂ ·2H ₂ O	3	0.735 g
MgCl ₂ ·6H ₂ O	4	0.203 g
NaH ₂ PO ₄ ·H ₂ O	5	0.276 g
NaHCO ₃	6	0.168 g

We compared mineral formation from different concentrated (1x, 5x, 10x) SBF solutions under the same condition (7 days incubation, 37 °C, renew SBF every 24 hours). To compare precipitation thickness, a scanning microscope with a surface profiling function (Laser Scanning Microscope, Keyence VK-X100, Osaka, Japan) was used to evaluate the thickness difference between the precipitated area and the masking area.

The result is shown in Fig. 13. A higher concentrated SBF solution can precipitate more minerals in the same period. As the SBF solution is more supersaturated, higher ion concentration will lead to more reactions once the mineralization process has been started. This tendency is also consistent with a previous study by Hata et al. ^[34], who studied a lower concentration range (concentration between 0.5x to 1.5x).

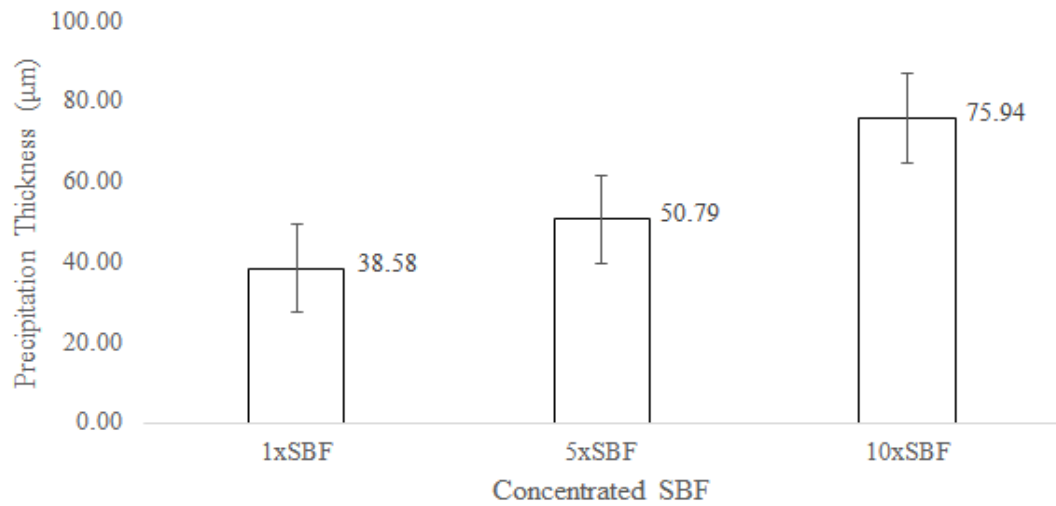


Fig. 12 Mineral layer thickness on the same substrate soaked in different concentrated simulated body fluids for the same period.

It also has been noticed that there are different definitions of concentrated SBF solution (such as only keeping Ca^{2+} ions in proportion or keeping both Ca^{2+} and PO_4^{2-} in proportion). In our study, we defined the concentration of SBF based on the

concentration of Ca^{2+} because $\text{CaCl}_2 \cdot 2\text{H}_2\text{O}$ can release all Ca^{2+} in solution. Compared to Ca^{2+} , there are multiple balances related to PO_4^{2-} , which is difficult to confirm the final concentration of PO_4^{2-} without any instrument.

3.3 pH Value

We also monitored the pH variation with the time for mineralization in highly concentrated SBF solutions such as 10x SBF. As we mentioned previously, some revised recipes of SBF we used did not include chemicals like Tris to construct a buffer system in the solution. With the buffer system constructed, the pH of the solution can be kept in a certain range [35]. In SBF, a stable pH value means the supersaturated status can be maintained so the SBF can keep functioning. Thus, there is no need to refresh the solution in the incubator. However, many of our highly concentrated SBF were not buffer solution systems. Thus, we need to study how long the highly concentrated SBF can function to decide the necessity and time point of refreshing.

To learn more about pH variation in highly concentrated SBF, we prepared a 10x SBF solution for testing. The pH value was measured every 10 min in the first hour and then was measured every hour by a pH meter (Extech PH220-C). Room temperature and relative humidity were also recorded at the same time in case they have any influence on the mineralization. The result is shown in Fig. 14. It can be seen that the pH of the SBF solution was increasing slowly and reached the highest value after 5 hours but the solution was still clear. Then, it dropped relatively fast and the solution became cloudy. After 9 hours, the final pH value was maintained stable and was lower than the initial pH value.

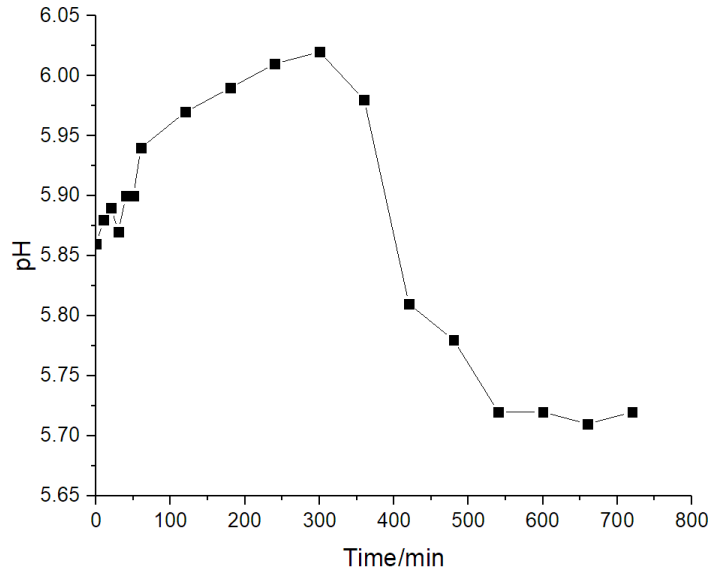


Fig. 13 pH variation in 12 hours and illustrations of typical phenomena at different stages. Temperature and relative humidity are consistent.

The experiment showed that the 10x SBF without buffer system lost its functionality in less than a day. The final pH value was below the pH right after preparation, which indicates that the status of this solution system may no longer be supersaturated. If we would like to conduct experiments by using the SBF without buffer, the simplest way is to refresh the solution daily. Or, we could search for other chemicals that can build a buffer system suitable for maintaining the pH around this level.

3.4 Conclusion

In this chapter, we studied factors and conditions involved in the mineralization process from simulated body fluids. We compared our measurement results of our piezoelectric samples to the reference value provided by the manufacturer. We also compared the precipitated mineral thickness produced from different recipes of simulated body fluids in previous studies. The result demonstrated that more minerals

can be deposited from higher concentrated minerals. However, the pH varies dramatically in the highly concentrated SBF solution because it usually does not contain any chemicals to build a buffer system, which requires a daily refresh of the solution if used for an experiment lasting longer than one day.

Chapter 4

Characterizations of Bioinspired Composites

4.1 Surface Morphology

When studying factors that influence composite synthesis, we noticed several different types of morphologies of deposited minerals on the surface. Previous studies from Sadat-Shojai ^[36] and Dorozhkin ^[37] et al. showed that calcium phosphates can form many unique types of morphologies under specific methods of synthesis. Currently well-known and discovered shapes are irregular spheres (Fig. 15a), spheres (Fig. 15b), flowers (Fig. 15c), porous spheres (Fig. 15d), bowknots (Fig. 15e), dumbbells (Fig. 15f), needles (Fig. 15g), sheets (Fig. 15h), self-assembled nanorods (Fig. 15i), rosettes (Fig. 15j), and flakes (Fig. 15k), as shown in Fig. 15. Among these morphologies, irregular spheres (Fig. 15a), spheres (Fig. 15b), flowers (Fig. 15c), dumbbells (Fig. 15f), needles (Fig. 15g), sheets (Fig. 15h), self-assembled nanorods (Fig. 15i), and flakes (Fig. 15k), are common shapes formed when synthesizing by

conventional chemical precipitation method based on reactions between reagents containing calcium and phosphate in solvents.

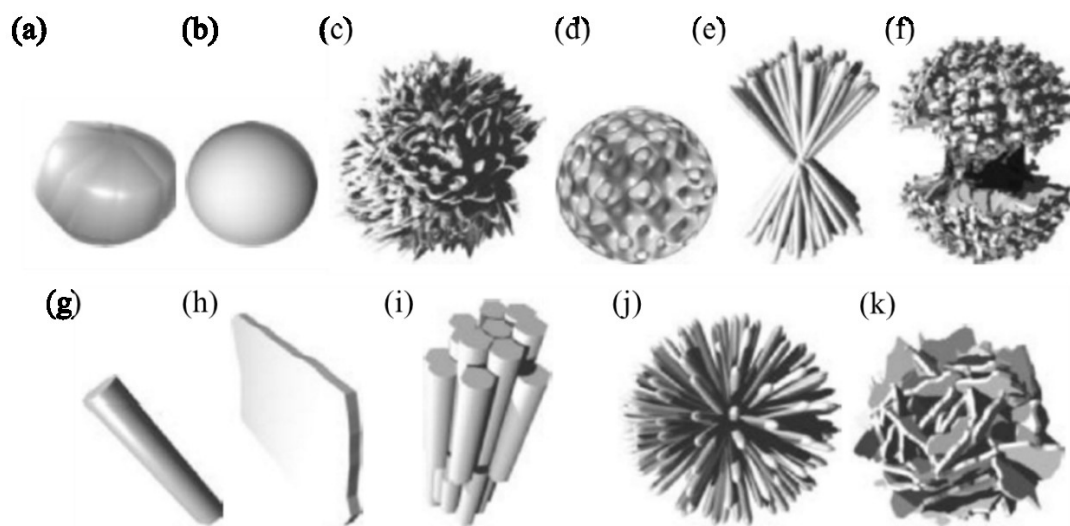


Fig. 14 Common morphologies of calcium phosphate researchers have discovered. These shapes are (a) irregular spheres, (b) spheres, (c) flowers, (d) porous spheres, (e) bowknots, (f) dumbbells, (g) needles, (h) sheets, (i) self-assembled nanorods, (j) rosettes, and (k) flakes. Reprinted from *Acta biomaterialia*, 9(8), 7591-7621,^[36] with permission from Elsevier.

The morphologies shown in our minerals are dense spherical and flaky shapes (Fig. 16b, Fig. 16d), corresponding to previous studies (Fig. 15b, Fig. 15k). We also compared our minerals with other results where researchers induced mineral precipitation from a similar chemical system on different material surfaces with charges by using scanning electron microscopy. Our deposited mineral layer shared the similar morphology with previous studies (Fig. 16) from Kokubo et al.^[20], Li et al.^[38], and Kobayashi et al.^[39]. However, accurate analysis of chemical components should be tested to obtain detailed information and provide a better understanding.

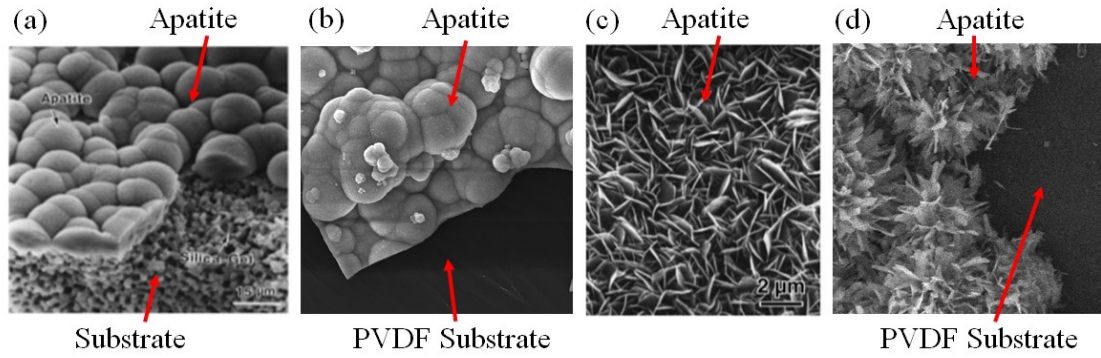


Fig. 15 (a) Dense spherical mineral layer observed in previous studies from Kokubo et al. and Li et al.; (b) Dense spherical mineral layer observed in our study share the same morphology; (c) Flaky-shape mineral layer shown in previous research from Kobayashi et al. and Li et al; (d) Flaky-shape mineral layer shown in our study also has been discovered. Reprinted from *Biomaterials*, 27(15), 2907-2915,^[20] with permission from Elsevier.

4.2 Chemical Composition Analysis

While morphology is related to chemical composition, calcium phosphates can have different kinds of morphologies based on factors such as ion concentration, pH, reaction temperature, aging temperature, aging duration, and drying method, etc.^[36] Thus, to further confirm the component of precipitated minerals, more characterization methods should be applied.

To characterize the composition of minerals, we analyzed the precipitated minerals with an X-ray diffractometer (X'Pert, for powder, Cu K-radiation: 40 kV, 40 mA, scanning range: 10° to 70°, step size: 0.05°). It can provide the structure of materials to identify compounds based on their diffraction patterns^[40].

Minerals were collected from PVDF film samples with static loading in the 10x SBF solution system. The analyzed result is shown in Fig. 17. We compared our result with a standard XRD diagram of hydroxyapatite and noticed that the peaks from deposited minerals showed a good match with those from hydroxyapatite, one form of calcium phosphates, which is the main mineral component of bone^[11]. Main peaks

were correlated with those from the hydroxyapatite though, due to background noise, some small peaks could not be distinguished clearly.

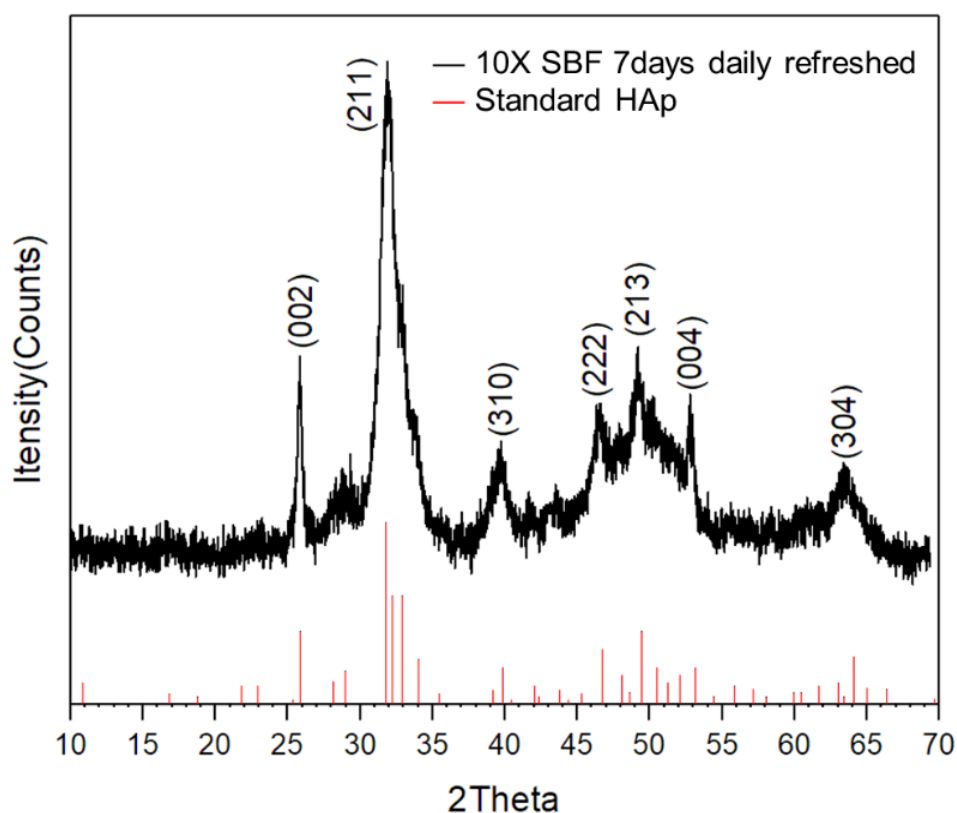


Fig. 16 XRD analysis of deposited minerals on PVDF substrate

Beside XRD, we also analyzed precipitated minerals with energy dispersive spectroscopy (EDS; EDAX Co., USA, Octane Plus) on the scanning electron microscope (SEM; Tescan, Mira3). The EDS can perform an elemental analysis of samples. After stimulating atoms in the sample, it can recognize elements existing in the sample based on their unique emission spectra decided by the atomic structure ^[41]. The analyzed results are shown in Fig. 18. For samples from differently concentrated SBF solutions, calcium (Ca), phosphorus (P), and oxygen (O) elements were detected with relatively high ratio, which are the elements consisting of hydroxyapatite. For 1xSBF, due to limited mineral coverage, carbon (C) and fluorine (F) peaks from the

underlying PVDF substrates were also detected. Some small peaks from sodium or other elements can also be obtained occasionally after rinsing with DI water, especially in higher concentrated solutions, which are from remaining NaCl due to their high concentrations.

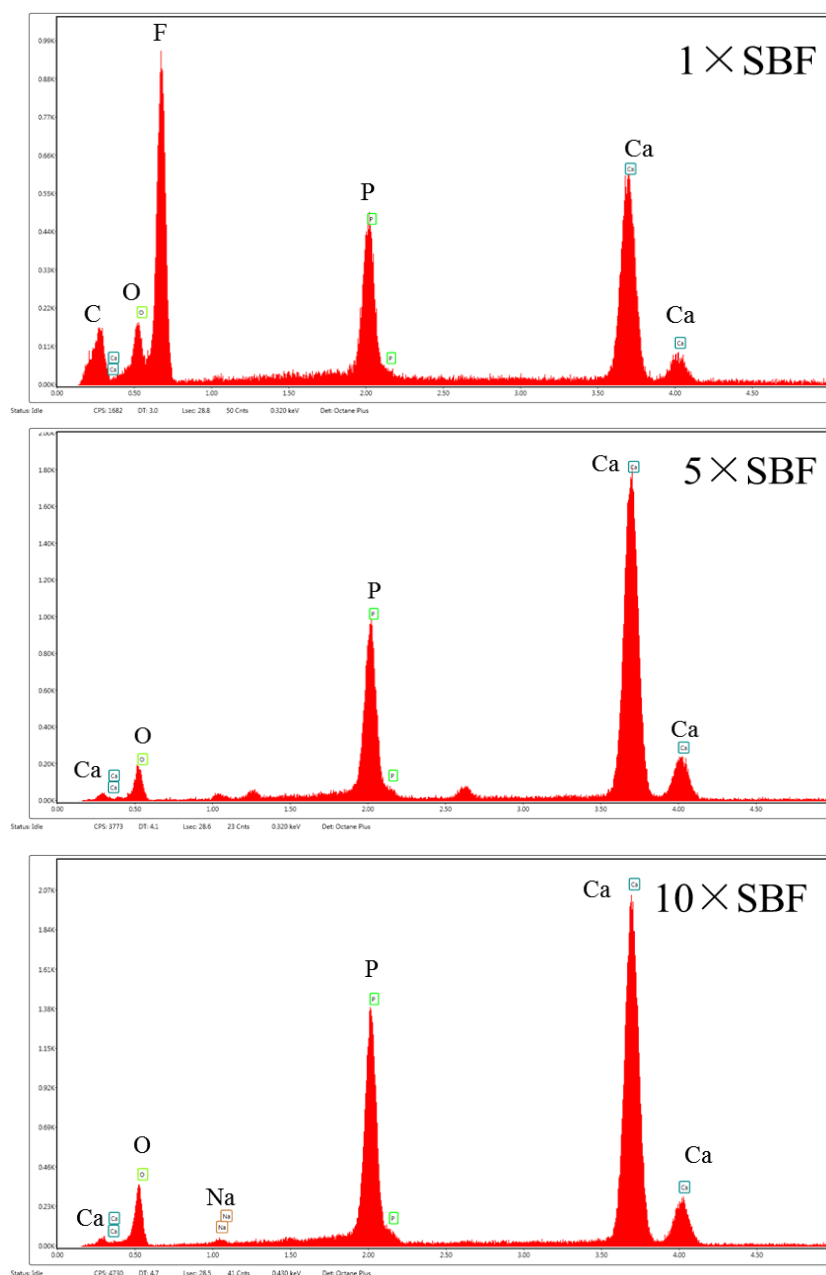


Fig. 17 EDS analysis of chemical elements in the deposited mineral layer formed from 1x, 5x, 10x simulated body fluids separately.

4.3 Testing Regeneration of Damaged Areas

We also tested the regeneration capability of the composite when damages appeared. As the damaged regions expose the negative charges on the surface, the material system might be able to repair damages by precipitating minerals on the damaged sites from the SBF.

For testing, PVDF film samples were prepared with well-defined geometries and were immersed into SBF for mineral formation at room temperature without loading. Then, parts of the mineralized surfaces were damaged with wires and the damaged specimens were immersed into the SBF solution again as shown in Fig. 19 and were checked periodically. (Fig. 19)

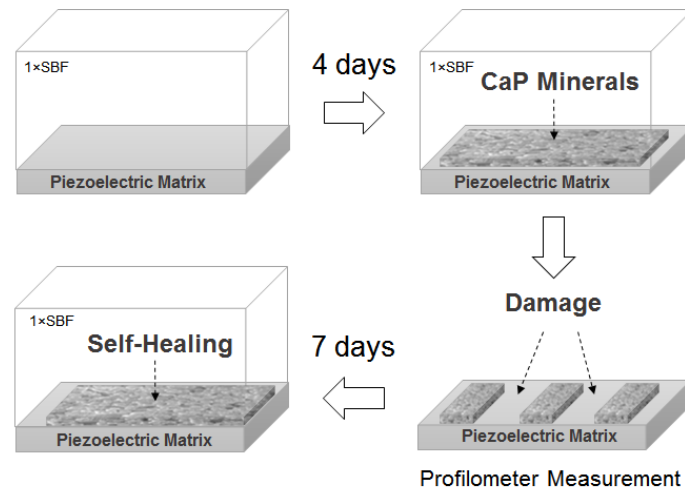


Fig. 18 Schematic of testing regeneration of damaged areas.

The result is shown in Fig. 20 from optical microscope images. Minerals were deposited onto damaged regions due to the exposure of negative charges on the PVDF film substrates while there was a small amount of minerals deposited onto the remaining regions due to the existing layers.

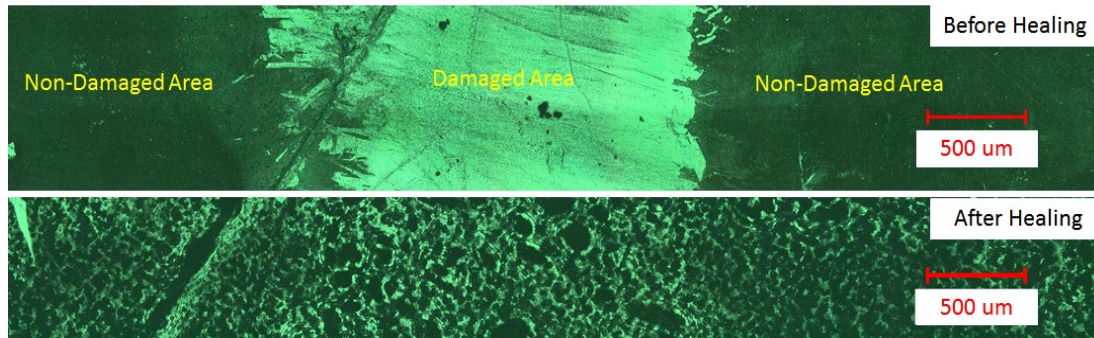


Fig. 19 An overview of the sample after damage (Top) and after healing (Bottom).

We also scanned and analyzed the damaged and non-damaged areas by non-contact profilometer (Laser Scanning Microscope, Keyence VK-X100, Osaka, Japan), to measure the thickness profiles of deposited minerals on PVDF films. Before scanning, samples were carefully attached to a silicon wafer by a tape. Samples were scanned with a 20× objective lens. The profilometer collected 3D information from the scanned area. Images were stitched together in all scanned areas to synthesize the final result.

Scanning results were first processed by the VK analysis application (Keyence, Osaka, Japan) to correct obvious surface tilting by checking the level of the substrate layer. Common correction methods used were the 2-point linear profile correction and the 3-point non-linear profile correction, depending on specific situations. Later, the Gwyddion (Department of Nanometrology, Czech Metrology Institute) was used to process the measured data. The 3D reconstruction can be obtained both by VK analysis application and Gwyddion to check scanning qualities. To measure the thickness variation along one direction, line width (line thickness) was set to proper (such as 15-20) pixels to suppress influence from background noise and enlarge the sampling area.

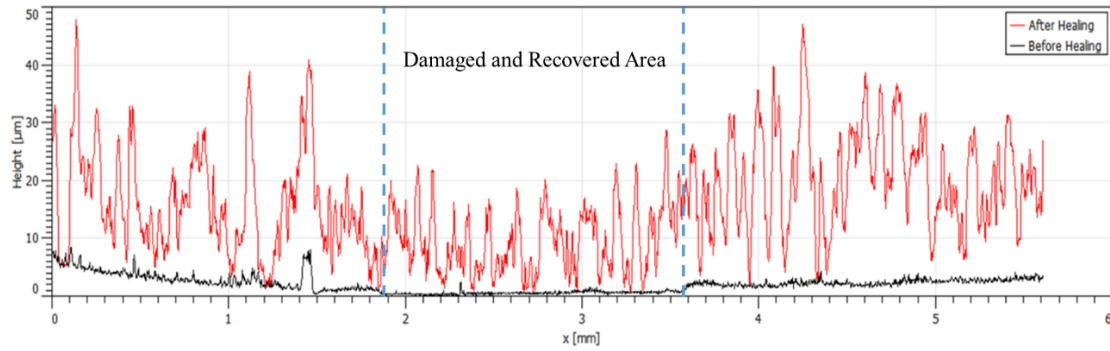


Fig. 20 Thickness measurement of the damaged area and non-damage area after damage (Black) and after healing (Red)

The scanning result (Fig. 21) shows that mineral growth occurred when we immersed back to SBF after damage both on damaged and non-damaged areas. More minerals were deposited compared to the initial synthetic process. Though minerals covered the damaged area again, the damaged area had a thinner layer than that of the non-damaged area. The preliminary data suggest that while the material system can regenerate damaged areas, the mineralization does not seem to selectively occur in only damaged areas. One of the possible reasons is the existing minerals in the non-damaged area can lower the energy for nucleation and growth while the exposure of charges in the damaged areas can facilitate nucleation.

4.4 Conclusion

In this chapter, we mainly focus on the characterizations of precipitated minerals. Several methods have been applied including optical microscope to measure the surface morphology as well as XRD and EDS to analyze the chemical structure and element. The results suggest that the deposited minerals are hydroxyapatite, one type of calcium phosphate. Moreover, our studies showed that the material system can regenerate damages while it might not selectively induce mineralization only on damaged areas.

Chapter 5

Conclusion and Future Work

5.1 Summary of Current Work

Based on previous findings that negatively charged scaffolds serve as templates for mineral formation from the medium with ions by attracting positive mineral ions, we demonstrated the regeneration capability of our bioinspired composites after a series of studies related to inducing mineralization from simulated body fluids (SBF) on the surface of PVDF film.

Firstly, we studied the piezoelectricity of PVDF film under compression, mimicking a mechanical situation when damage was applied. The PVDF samples we prepared showed their d_{33} values at a range around 20pC/N to 35pC/N, which is close to the reference value provided by the manufacturer, 33pC/N. We then studied the influence of SBF on mineral deposition thickness with 1xSBF, 5xSBF, and 10xSBF. Our results showed that more minerals can be deposited from highly concentrated SBF. We examined the precipitated minerals mainly by XRD and EDS, and the analysis

results indicated that the deposited minerals are hydroxyapatite, one form of calcium phosphate, which is the main inorganic materials in bones. We finally explored the regeneration capability of our bioinspired composite and noticed that the damaged mineral layer on the negatively charged surface of PVDF film was recovered after re-immersing into simulated body fluids. The result seems to be consistent with our hypothesis that the damage of the mineralized scaffold will expose underlying negative charges so that it can provide “signals” for inducing mineral deposition, thus repairing the damaged mineral layer.

5.2 Future Work

There are still many aspects to study in the future. In terms of the mechanism, we still do not have a straightforward method to observe and monitor the beginning of mineral deposition for verifying our mechanism based on nucleation and growth. In the future, a cryo-SEM could be used to observe frozen samples at different time points from the mineralization process, followed by EDS analysis on the frozen cross-section of the solution, to obtain the distribution of chemical elements in SBF.

Besides, when studying regeneration capability, we also noticed that there is a mineral growth in the non-damaged area, and it seems that there still has a thickness difference after recovery. More quantitative studies should be conducted to measure the thickness increase per day and analyze the deposition rate on the damaged and non-damaged area from the beginning of regeneration.

In the future, it is also necessary to combine biocompatibility with previously studied materials with regeneration capability for future medical implants because some

of these materials can have unique performance during regeneration, such as preventing crack expansion, the high recovery rate in mechanical properties, etc.

5.3 Perspectives of Our Bioinspired Composite

We envision that the findings from our research can contribute to new strategies for various areas including coatings for medical implants, teeth/bone remineralization, and scaffolds. Since our regeneration strategy is based on a biocompatible environment, the recovery process does not contain cytotoxic materials and does not require extreme conditions where an organism cannot survive. Another benefit is that materials with regeneration ability can lower the cost and risk for maintenance and simplify the repairing process, especially for medical implants. Moreover, since bioinspired composites with regeneration ability do not rely on a biological process, they could be suitable for many uses.

Bibliography

- [1] Ferguson, C. (2006). Historical Introduction to the Development of Material Science and Engineering as a teaching discipline. available from the UKCME at <http://www.materials.ac.uk/pub/Materials-History-Intro.pdf>.
- [2] Cohen, M. (1974). Materials and Man's Needs. Summary Report of the Committee on the Survey of Materials Science and Engineering, Washington: National Academy of Science.
- [3] Wegst, U. G., Bai, H., Saiz, E., Tomsia, A. P., & Ritchie, R. O. (2015). Bioinspired structural materials. *Nature materials*, 14(1), 23.
- [4] Patrick, J. F., Robb, M. J., Sottos, N. R., Moore, J. S., & White, S. R. (2016). Polymers with autonomous life-cycle control. *Nature*, 540(7633), 363-370.
- [5] EPA, U. (2019). Advancing sustainable materials management: 2017 fact sheet.
- [6] Blaiszik, B. J., Kramer, S. L., Olugebefola, S. C., Moore, J. S., Sottos, N.

- R., & White, S. R. (2010). Self-healing polymers and composites. *Annual review of materials research*, 40, 179-211.
- [7] White, S. R., Sottos, N. R., Geubelle, P. H., Moore, J. S., Kessler, M., Sriram, S. R., ... & Viswanathan, S. (2001). Autonomic healing of polymer composites. *Nature*, 409(6822), 794.
- [8] Pang, J. W. C., & Bond, I. P. (2005). 'Bleeding composites'—damage detection and self-repair using a biomimetic approach. *Composites Part A: Applied Science and Manufacturing*, 36(2), 183-188.
- [9] Chen, X., Dam, M. A., Ono, K., Mal, A., Shen, H., Nutt, S. R., ... & Wudl, F. (2002). A thermally re-mendable cross-linked polymeric material. *Science*, 295(5560), 1698-1702.
- [10] Li, C. H., Wang, C., Keplinger, C., Zuo, J. L., Jin, L., Sun, Y., ... & You, X. Z. (2016). A highly stretchable autonomous self-healing elastomer. *Nature chemistry*, 8(6), 618.
- [11] Feng, X. (2009). Chemical and biochemical basis of cell-bone matrix interaction in health and disease. *Current chemical biology*, 3(2), 189-196
- [12] Bassett, C. A. L. (1967). Biologic significance of piezoelectricity. *Calcified tissue research*, 1(1), 252-272.
- [13] Noris-Suárez, K., Lira-Olivares, J., Ferreira, A. M., Feijoo, J. L., Suárez, N., Hernández, M. C., & Barrios, E. (2007). In vitro deposition of hydroxyapatite on cortical bone collagen stimulated by deformation-induced piezoelectricity. *Biomacromolecules*, 8(3), 941-948.

- [14] Rajabi, A. H., Jaffe, M., & Arinzeh, T. L. (2015). Piezoelectric materials for tissue regeneration: A review. *Acta biomaterialia*, 24, 12-23.
- [15] Yamashita, K., Oikawa, N., & Umegaki, T. (1996). Acceleration and deceleration of bone-like crystal growth on ceramic hydroxyapatite by electric poling. *Chemistry of materials*, 8(12), 2697-2700.
- [16] An, J., Leeuwenburgh, S., Wolke, J., & Jansen, J. (2016). Mineralization processes in hard tissue: bone. In *Biomineralization and Biomaterials* (pp. 129-146). Woodhead Publishing.
- [17] Liu, X., Ding, C., & Wang, Z. (2001). Apatite formed on the surface of plasma-sprayed wollastonite coating immersed in simulated body fluid. *Biomaterials*, 22(14), 2007-2012.
- [18] Navarro, M., & Serra, T. (2016). Biomimetic mineralization of ceramics and glasses. In *Biomineralization and Biomaterials* (pp. 315-338). Woodhead Publishing.
- [19] Kokubo, T., Kushitani, H., Sakka, S., Kitsugi, T., & Yamamuro, T. (1990). Solutions able to reproduce in vivo surface-structure changes in bioactive glass-ceramic A-W3. *Journal of biomedical materials research*, 24(6), 721-734.
- [20] Kokubo, T., & Takadama, H. (2006). How useful is SBF in predicting in vivo bone bioactivity?. *Biomaterials*, 27(15), 2907-2915.
- [21] Yang, F., Wolke, J. G. C., & Jansen, J. A. (2008). Biomimetic calcium phosphate coating on electrospun poly (ϵ -caprolactone) scaffolds for bone

tissue engineering. Chemical Engineering Journal, 137(1), 154-161.

- [22] Chou, Y. F., Chiou, W. A., Xu, Y., Dunn, J. C., & Wu, B. M. (2004). The effect of pH on the structural evolution of accelerated biomimetic apatite. Biomaterials, 25(22), 5323-5331.
- [23] Dove, P. M., De Yoreo, J. J., & Weiner, S. (2003). Biomineralization, Mineralogical Society of America. Washington, DC.
- [24] APC International, Ltd. (2002). Piezoelectric ceramics: principles and applications. APC International.
- [25] Jaffe, B. (2012). Piezoelectric ceramics (Vol. 3). Elsevier.
- [26] Tong, C. (2019). Introduction to Materials for Advanced Energy Systems. Springer.
- [27] Martins, P., Lopes, A. C., & Lanceros-Mendez, S. (2014). Electroactive phases of poly (vinylidene fluoride): Determination, processing and applications. Progress in polymer science, 39(4), 683-706.
- [28] Liu, F., Abed, M. M., & Li, K. (2011). Preparation and characterization of poly (vinylidene fluoride)(PVDF) based ultrafiltration membranes using nano γ -Al₂O₃. Journal of membrane science, 366(1-2), 97-103.
- [29] Safarpour, M., Khataee, A., & Vatanpour, V. (2014). Preparation of a novel polyvinylidene fluoride (PVDF) ultrafiltration membrane modified with reduced graphene oxide/titanium dioxide (TiO₂) nanocomposite with enhanced hydrophilicity and antifouling properties. Industrial & Engineering Chemistry Research, 53(34), 13370-13382.

- [30] Barooghi, B., Sheikhi, M., & Amiri, A. (2018). Effect of nano-hydroxyapatite and duty cycle on the structure and corrosion performance of plasma electrolyte oxidation coatings in simulated body fluid on Ti–6Al–4 V. *Proceedings of the Institution of Mechanical Engineers, Part C: Journal of Mechanical Engineering Science*, 232(23), 4229-4236.
- [31] N. Soin, S.C. Anand, T.H. Shah, 12 - Energy harvesting and storage textiles, Editor(s): A. Richard Horrocks, Subhash C. Anand, *Handbook of Technical Textiles (Second Edition)*, Woodhead Publishing, 2016, Pages 357-396, ISBN 9781782424659, <https://doi.org/10.1016/B978-1-78242-465-9.00012-4>.
- [32] Stewart, M., & Cain, M. G. (2014). Direct piezoelectric measurement: The berlincourt method. In *Characterisation of Ferroelectric Bulk Materials and Thin Films* (pp. 37-64). Springer, Dordrecht.
- [33] Stewart, M., Battrick, W., & Cain, M. G. (2001). Measuring piezoelectric d33 coefficients using the direct method.
- [34] Hata, K., Kokubo, T., Nakamura, T., & Yamamuro, T. (1995). Growth of a bonelike apatite layer on a substrate by a biomimetic process. *Journal of the American Ceramic Society*, 78(4), 1049-1053.
- [35] Stoll, V. S., & Blanchard, J. S. (1990). [4] Buffers: Principles and practice. In *Methods in enzymology* (Vol. 182, pp. 24-38). Academic Press.
- [36] Sadat-Shojai, M., Khorasani, M. T., Dinpanah-Khoshdargi, E., & Jamshidi, A. (2013). Synthesis methods for nanosized hydroxyapatite with diverse

structures. *Acta biomaterialia*, 9(8), 7591-7621.

- [37] Dorozhkin, S. V. (2016). Calcium orthophosphates (CaPO₄): occurrence and properties. *Progress in Biomaterials*, 5(1), 9-70.
- [38] Kobayashi, T., Ono, S., Hirakura, S., Oaki, Y., & Imai, H. (2012). Morphological variation of hydroxyapatite grown in aqueous solution based on simulated body fluid. *CrystEngComm*, 14(3), 1143-1149.
- [39] Li, N. B., Xu, W. H., Zhao, J. H., Xiao, G. Y., & Lu, Y. P. (2018). The significant influence of ionic concentrations and immersion temperatures on deposition behaviors of hydroxyapatite on alkali-and heat-treated titanium in simulated body fluid. *Thin Solid Films*, 646, 163-172.
- [40] Hanawalt, J. D., Rinn, H. W., & Frevel, L. K. (1938). Chemical analysis by X-ray diffraction. *Industrial & Engineering Chemistry Analytical Edition*, 10(9), 457-512.
- [41] Ebnesajjad, S., & Ebnesajjad, C. (2013). Surface treatment of materials for adhesive bonding. William Andrew.
- [42] Moheimani, S. R., & Fleming, A. J. (2006). Fundamentals of piezoelectricity. *Piezoelectric transducers for vibration control and damping*, 9-35.
- [43] Mishra, S., Unnikrishnan, L., Nayak, S. K., & Mohanty, S. (2019). Advances in piezoelectric polymer composites for energy harvesting applications: A systematic review. *Macromolecular Materials and Engineering*, 304(1), 1800463.

Biography

Decheng Hou was born in 1994 in the People's Republic of China.

Decheng did his undergraduate work at Tsinghua University, Beijing, China, where he majored in Mechanical Engineering. During his undergraduate studies, he spent a year designing a V-type mixer for Material Science Laboratory, a month in Pohang University of Science and Technology learning microfabrication and lab-on-a-chip for cells, and another year in biofabrication of a contractile and highly elastic vessel-like structure as his graduation project. He also joined Zhangli Peng's group at the University of Notre Dame as a research assistant in the International Student Research Experience (iSURE) Program in the summer of 2016, studying multiscale modeling of cells.

In 2017, Decheng began his master at Johns Hopkins University. He was a teaching assistant for Profs. Steven P. Marra's Thermal Dynamic Lab class and Sung H. Kang's Fabricatology class, and a research assistant in the Hopkins Extreme Materials Institute (HEMI).